Direct measurements of air layer profiles under impacting droplets using high-speed color interferometry

Roeland C. A. van der Veen, Tuan Tran,* Detlef Lohse,† and Chao Sun‡
Physics of Fluids, University of Twente, P.O. Box 217, 7500 AE Enschede, The Netherlands
(Received 15 November 2011; published 23 February 2012)

A drop impacting on a solid surface deforms before the liquid makes contact with the surface. We directly measure the time evolution of the air layer profile under the droplet using high-speed color interferometry, obtaining the air layer thickness before and during the wetting process. Based on the time evolution of the extracted profiles obtained at multiple times, we measure the velocity of air exiting from the gap between the liquid and the solid, and account for the wetting mechanism and bubble entrapment. The present work offers a tool to accurately measure the air layer profile and quantitatively study the impact dynamics at a short time scale before impact.

DOI: 10.1103/PhysRevE.85.026315 PACS number(s): 47.55.nd, 47.20.Ma, 47.55.D−

I. INTRODUCTION

Drop impact on solid surfaces, aside from its inherent beauty, has been playing an increasingly important role in industrial processes as diverse as ink-jet printing, spray cooling, and spray coating. Since it was studied in 1876 by Worthington [1], the phenomenon has received tremendous attention from researchers, yet our understanding of this subject is still far from being complete (see review article [2]). A challenge in studying this problem arises from widely different time and spatial scales of the involved effects. Another difficulty comes from determining relevant physical parameters that govern the impact dynamics. For example, beside apparent parameters such as the surface roughness and wettability, the liquid viscosity, surface tension, and density, it was recently discovered that the ambient pressure is also a crucial parameter as it dictates the splash threshold after impact [3]. This finding and subsequent studies [4–6] suggest that the air layer between an impinging droplet and a solid surface may have significant effects on the impact's outcomes. Hence, it is essential to understand how the drop and the surface interact through the air layer.

On the theoretical side, a mechanism of splash formation focusing on the short time scale within which the drop starts to be deformed has been proposed [7,8]. Detailed analysis and simulations have been subsequently developed [9,10]. On the experimental side, the dynamics of droplet impact at the earliest time scale have also been studied; one of the most remarkable phenomena is the detection of entrapped bubbles under an impacting drop [11–14]. The existence of these bubbles indicates that the drop's bottom surface is deformed before it makes contact with the surface. There is, however, a lack of detailed measurements of the air layer thickness at the earliest time of impact, as well as the formation of the entrapped bubbles.

Here we report the direct measurement of the evolution of the air layer profile between an impinging droplet and a solid surface using high-speed color interferometry. This method has been successfully applied to measure the vapor layer profile between an impinging droplet and superheated surfaces (see Ref. [15] for the detailed results). In this paper, we focus on the earliest time of impact when the liquid has not touched the surface but starts to be deformed due to the pressure increase in the air layer between the liquid and the solid surface. We measure the air flow between the droplet and the solid surface and investigate the mechanism of bubble entrapment.

II. EXPERIMENTS

In Fig. 1(a) we show a schematic of the experimental setup for the present work. We generate liquid drops by using a syringe pump to push liquid out of a fine needle. The drop detaches as soon as its weight overcomes the surface tension and then falls on a microscope glass slide (Menzel microscope slide, average roughness ≈10 nm). In our experiments, the working liquid is milli-Q water (density $\rho_w = 998\,\mathrm{kg/m^3}$, surface tension $\sigma_w = 72 \times 10^{-3}$ N/m, viscosity $\nu_w = 10^{-6}\,\mathrm{m^2/s}$). The drop typically has diameter $D \approx 2$ mm and its velocity before impacting the surface can be adjusted by varying the needle's height H. We capture the drop impact from the bottom with a color high-speed camera (SA2, Photron Inc.) connected to a long-working-distance microscope (Navitar Inc.) and a 5× objective. The field of view achieved by this combination is 2 mm. We illuminate the impact area from below by supplying white light from a high-intensity fiber lamp (Olympus ILP-1) to the microscope's coaxial light port. When a drop approaches the glass slide, a thin film of air is formed between the liquid and solid surfaces before wetting occurs. Light of the same wavelength coming from the bottom, upon reflection from both surfaces of the film [Fig. 1(b)] forms interference patterns recorded by the camera. Each one of these patterns consists of constructive (bright) and destructive (dark) fringes; the fringe spacing depends on the air layer thickness and the wavelength of incident light. Since the lamp emits light of multiple wavelengths, the superposition of all available patterns produces concentric rings of rainbow colors as shown in Fig. 1(c).

In most of our experiments, we set the camera's frame rate to 10000 frames per second (FPS), and its resolution to 512 × 512 pixels to capture droplets with impact velocity less

*t.tran@utwente.nl
†d.lohse@utwente.nl
‡c.sun@utwente.nl

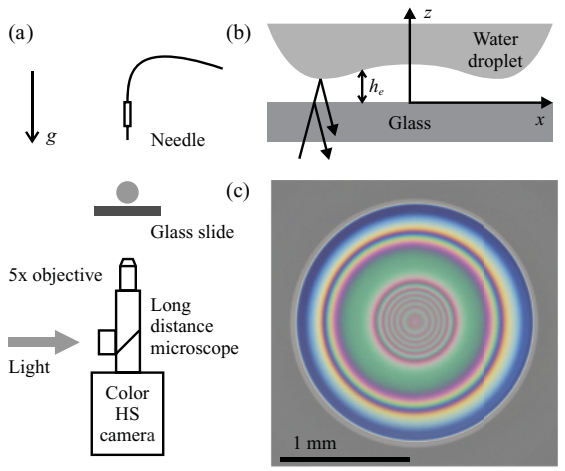

FIG. 1. (Color online) (a) Schematic of the experimental setup (not drawn to scale) used to study droplet impact on smooth surfaces. A water droplet of initial diameter $D_0 \approx 2$ mm falls on a glass slide of average roughness 10 nm. The bottom view is captured by a high-speed color camera (SA2, Photron Inc.). The camera is connected to a long-working-distance microscope and a 5× objective to obtain a 2-mm field of view. (b) Schematic of the air film between the drop and the glass slide (not drawn to scale). Light is supplied from the bottom for illumination; reflection of light from the upper surface of the glass slide and from the bottom surface of the drop causes interference fringes captured with the color camera. (c) An example of an interference pattern.

than 0.5 m/s. In the case that the impact velocity is higher, the frame rate can be set as high as 86400 FPS at resolution 32×256 pixels to capture the impact dynamics.

III. METHODS

In order to extract the absolute thickness of the air layer between an impinging drop and a glass surface, we construct a set of reference colors that can be related to absolute thickness. We put a convex lens on top of the glass slide [see inset in Fig. 2(b)] and observe the interference rings caused by the air film between two surfaces. Since the pattern consists of concentric rings of different colors and the air film thickness is known at each radial location, each color along a line passing through the center of these rings is associated with a thickness value. In Fig. 2(b) we show the air thickness profile between the lens and the glass slide. The color variation due to change in air thickness is obtained by taking a thin radial strip of 100×2200 pixels from an image of an interference pattern and then averaging colors in the transverse direction to reduce noise. The resulting strip [Fig. 2(a)], which has no color variation in the transverse direction, contains $N = 2200$ pixels in the x direction and hence N reference colors that can be used for calibration. Since the camera uses the sRGB model to represent colors, the color of each pixel i is represented by a color vector (R_i, G_i, B_i). The pixel's coordinate is x_i, which is related to a value of thickness h_r^i. Thus, we have a set of reference colors (R_i, G_i, B_i) for $1 \leqslant i \leqslant N$, each of which is associated with a reference thickness h_r^i. The reference thickness range is $0 \leqslant h_r^i \leqslant 4\,\mu$m. The thickness-color relation is shown in Fig. 2(c).

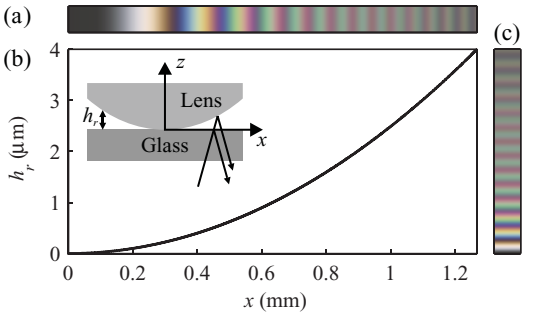

FIG. 2. (Color online) (a) Reference thickness of the air film between a lens and a glass slide. The lens has radius of the surface in adjacent with the glass $R = 200$ mm. Inset: schematic of the setup used to calibrate colors. (b) Color variation in the radial direction of the interference pattern used to calibrate colors. (c) Relation between thickness and reference colors.

The sRGB model, however, is generally not preferred when comparing colors between experiments because it does not decouple light intensity and color information, which poses a problem due to variations in illumination conditions such as light intensity, incident, and observing angles. Instead, we use the CIE 1976 color model (also called CIELAB), a model that is most effective in decoupling light intensity [16] (see Appendix A for details). To work with colors in the CIELAB color space, we convert sRGB-format images to the absolute color space (XYZ) and then to CIELAB [16]. A color in the CIELAB model has three components: $\boldsymbol{L}$ for lightness information, and $\boldsymbol{a}$ and $\boldsymbol{b}$ for color information. Thus, we can separate light intensity from our analysis by omitting the component $\boldsymbol{L}$. Each reference color i after intensity decoupling is represented by a two-component vector $(\boldsymbol{a}_r^i, \boldsymbol{b}_r^i)$ and is associated with a value of reference thickness h_r^i for $1 \leqslant i \leqslant N$ and h_r^i is in the range $0\,\mu\text{m} \leqslant h_r^i \leqslant 4\,\mu$m.

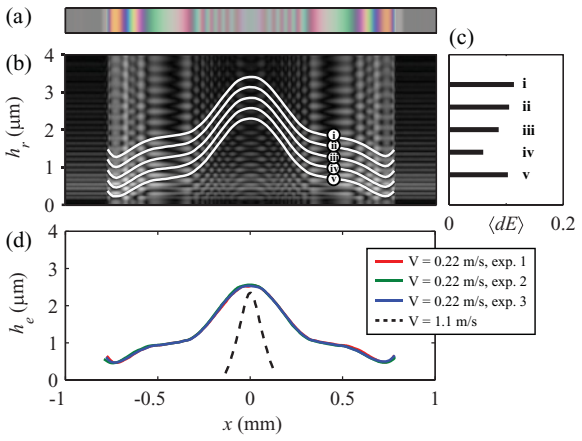

FIG. 3. (Color online) (a) Color sample of interference pattern taken at $t = 1.67$ ms after the bottom-view camera detected the drop. (b) Color difference in grayscale computed by Eq. (1) with candidate profiles shown in white solid lines. (c) Average color difference of candidate profiles shown in (b). (d) Solid lines: profiles computed from three different experiments with $V = 0.22$ m/s. Dashed line: $V = 1.1$ m/s. Note the extremely different length scales at the x axis (mm) and h_r axis (μm) in (b) and (d).

In Fig. 3(a) we show a color sample, which was taken along a diameter of an interference pattern under a drop with impacting velocity $V = 0.22\,\mathrm{m/s}$. After converting the color of each pixel to CIELAB color space and decoupling light intensity, we calculated the color difference dE^{ij} for each color $(\boldsymbol{a}_e^j, \boldsymbol{b}_e^j)$ in the sample $(1 \leqslant j \leqslant M = 596)$ and each reference color $(\boldsymbol{a}_r^i, \boldsymbol{b}_r^i)$ using the Euclidean distance

$$dE^{ij} = \left[\left(\boldsymbol{a}_e^j - \boldsymbol{a}_r^i\right)^2 + \left(\boldsymbol{b}_e^j - \boldsymbol{b}_r^i\right)^2\right]^{1/2}, \tag{1}$$

for $1 \leqslant i \leqslant N$ and $1 \leqslant j \leqslant M$. Since each color $(\boldsymbol{a}_e^j, \boldsymbol{b}_e^j)$ is associated with a coordinate x_j and, recalling that each reference color $(\boldsymbol{a}_r^i, \boldsymbol{b}_r^i)$ is associated with a value of reference thickness h_r^i, the color difference dE^{ij} can be thought of as a function of h_r^i and x_j. In Fig. 3(b) we show a plot of dE^{ij} in grayscale for $1 \leqslant i \leqslant N$ and for $1 \leqslant j \leqslant M$. The range of the index i translates to the range of reference thickness $0 \leqslant h_r \leqslant 4\,\mu\mathrm{m}$, and similarly to that of the index j to $-1 \leqslant x \leqslant 1\,\mathrm{mm}$. In the plot, black means $dE = 0$ and hence zero color difference, whereas white means the largest color difference. A vertical line at a particular value of x has all possible values of the film thickness at that point; the correct thickness value corresponds to the darkest point. In the case that there are multiple dark points on the same vertical line with insignificant difference between them, thickness determination is not trivial (see Appendix A for details). We note that, however, the film profile is continuous and smooth. Evidently, there are only a few continuous dark lines that can be distinguished without any abrupt change in slope. In Fig. 3(b) we show the candidate profiles in white solid lines [labeled from (i) to (v)]. The film thickness profile can be identified by considering the average color difference $\langle dE \rangle$ along each candidate profile L

$$\langle dE \rangle^L = \frac{1}{N_L} \sum_L dE^L, \tag{2}$$

where the sum is taken for all the pixels along the profile L and then divided by the number of pixels (N_L). In Fig. 3(c) we show $\langle dE \rangle^L$ for all profiles. The smallest color difference is along profile (iv) for which $\langle dE \rangle^{\mathrm{iv}} = 0.06$, whereas the second smallest one is along profile (iii) for which $\langle dE \rangle^{\mathrm{iii}} = 0.09$. As a result, we conclude that profile (iv) is the air layer profile. A test case of an air film with a known thickness profile shows that the accuracy of our method is within 40 nm (see Appendix B). To check the reproducibility we repeated the experiment several times and extracted the air thickness in each experiment at the same time. The computed profiles are shown in Fig. 3(d). Given the variations between experiments such as releasing time, drop size, surface properties, etc., the method gives remarkably consistent results.

IV. RESULTS AND DISCUSSION

In Fig. 4, we show interference patterns obtained during drop impact ($V = 0.22\,\mathrm{m/s}$ and $D = 2\,\mathrm{mm}$) and their corresponding thickness profiles of the air layer. We define $t = 0$ as the moment when the liquid completely wets the solid surface. From the first pattern detected by the camera ($t = -3.75\,\mathrm{ms}$), it is readily seen that a dimple is already formed, which means that the camera did not capture the entire deformation process of the drop's lower surface, probably due to limited coherence length of the light source used in the present experiment.

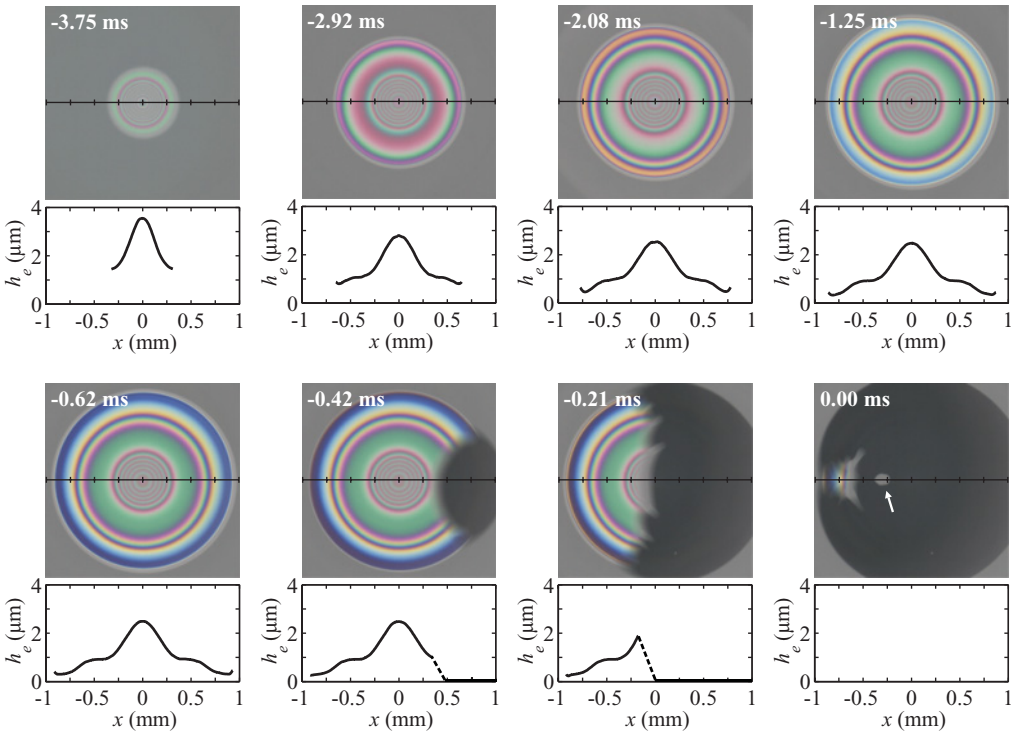

FIG. 4. (Color online) Snapshots of interference patterns obtained during drop impact and their corresponding calculated profiles ($V = 0.22\,\mathrm{m/s}$, $D = 2\,\mathrm{mm}$).

Subsequent profiles show that the dimple's height gradually reduces, while the liquid continues spreading in the radial direction. At $t = -0.42$ ms, the liquid starts wetting the glass surface at one point along the rim of the air layer and then propagates to the other side; the wetting process happens faster along the rim where the air thickness is smallest and finally traps air bubbles (indicated by an arrow at $t = 0$ ms). For experiments done under the same conditions, although the time that wetting occurs varies, we observe the same bubble-trapping dynamics, that is, the wetting front propagates faster at the rim and finally encloses the air pocket underneath the drop.

We note that there is a plateau (at $x \approx \pm 0.5$ mm) in the thickness profiles from $t = -2.92$ ms to $t = -0.21$ ms. This is due to the drop's oscillation as it falls down at a small distance from the surface (in this case $H = 6$ mm). When the drop detaches from the needle, capillary waves are generated and propagate to the other side. The surface deformation caused by these waves affects the dimple shape in addition to the pressure increase in the air layer under the drop. In the case that the drop is released from a greater height leaving sufficient time for viscosity to damp capillary waves, we do not observe the plateau in the thickness profiles. As shown in Fig. 3(d), the plateau is not present in the case of higher impact velocity case ($V = 1.1$ m/s, $H = 66$ mm).

We now quantify the velocity at the center of the dimple V_{dim} [inset of Fig. 5(a)]. As shown in Fig. 5(a), V_{dim} is found to be very small (roughly two orders of magnitude smaller) as compared to the impact velocity $V = 0.22$ m/s, which implies that the fluid at the bottom of the drop has decelerated before the camera starts capturing the interference fringes. Nonetheless, our measurements capture well the deceleration process of the lower surface of the drop from the detection point until it is brought to rest. Moreover, we estimate the horizontal velocity of air V_{air} based on the change in volume confined by a cylinder of radius R_C under the liquid surface [inset of Fig. 5(a)]. In Fig. 5(b) we show V_{air} at several values of R_C. The data show a consistent increase of the air velocity at a given time as it gets closer to the rim of the air layer where the thickness is minimum. For higher-impact velocity cases, the velocity of air is much higher due to the extremely thin air gap at the rim.

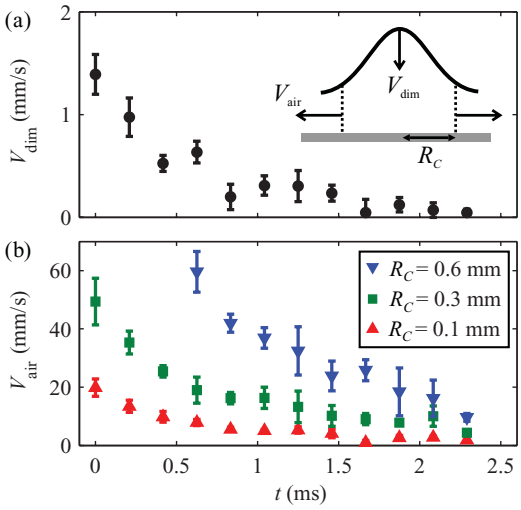

FIG. 5. (Color online) (a) Dimple velocity V_{dim} vs time. (b) The average velocity of air V_{air} vs time at different radial locations $R_C = 0.1$ mm (upward triangles), $R_C = 0.3$ mm (squares), $R_C = 0.6$ mm (downward triangles) for an experiment with impact velocity $V = 0.22$ m/s.

V. CONCLUSION

In conclusion, we have used high-speed color interferometry to measure the complete profile and its evolution of the air layer under an impacting drop for impact velocity $V = 0.22$ m/s and $V = 1.1$ m/s. From the experimental measurements, we account for the wetting mechanism, which results in entrapment of bubbles after impact. We also experimentally quantify the velocity of air flow between the drop and the surface, as well as the velocity of the dimple before wetting occurs. Our results offer a benchmark for theories of drop impact.

ACKNOWLEDGMENTS

This study was financially supported by the foundation for Fundamental Research of Matter (FOM) and the European Research Council ERC. The authors would like to acknowledge Markus Abel for useful discussions.

APPENDIX A: COLOR REPRESENTATION

The necessity of decoupling light intensity from color analysis leads us to resource the CIELAB model instead of the sRGB one. Here we present a test case comparing sRGB and CIELAB models. First we reduce light intensity in the interference pattern resulting from the calibration step by multiplying each channel of the RGB model by 0.75.

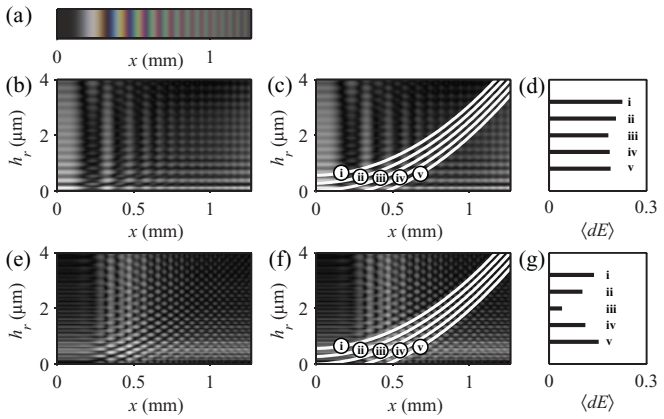

FIG. 6. (Color online) (a) Color variation (after reducing the intensity to 75%) depending on the air film thickness obtained in the calibration step. (b) sRGB model: color difference between the reference colors and the darkened ones in grayscale. (c) Candidate profiles resulting from the color difference in (b). (d) The averaged color differences along the candidate profiles shown in (c). (e) CIELAB model: color difference between the reference colors and the darkened ones in grayscale. (f) Candidate profiles resulting from the color difference in (e). (g) The averaged color differences along the candidate profiles shown in (f).

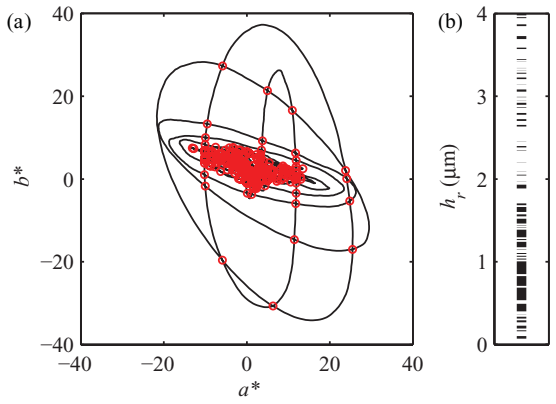

FIG. 7. (Color online) (a) Plot of reference color in $\boldsymbol{a}_r, \boldsymbol{b}_r$ space showing the color is not unique at some thickness values (red circles). (b) Only thickness values that have unique color are shown.

The darkened pattern is shown in Fig. 6(a). We use this pattern as a color sample from which air layer thickness is recovered. An image showing the color difference using sRGB representation in grayscale between the modified color set and the reference one is shown in Fig. 6(b). Clearly, without intensity decoupling, it is difficult to recover the air thickness profile. Even examining the average color difference along a few candidate profiles does not reveal which one is correct [Fig. 6(d)]. In contrast, the color sample after intensity decoupling with CIELAB model gives profiles with high contrast from the background [see Fig. 6(e)]. Figure 6(g) also shows that the correct one also has the smallest value of average color difference along candidate profiles in Fig. 6(f).

We now discuss an inherent issue of methods using color interferometry to measure film thickness regardless of color model, namely, repetition of colors at multiple values of film thickness [17]. We demonstrate this problem for the reference colors represented by the CIELAB model in Fig. 7(a). The plot shows $\boldsymbol{b}_r^i$ vs $\boldsymbol{a}_r^i$ for $1 \leqslant i \leqslant N$ and correspondingly $0 \leqslant h_r^i \leqslant 4\,\mu$m. Note that each pair of $(\boldsymbol{a}_r^i, \boldsymbol{b}_r^i)$ represents one color and is associated with a value of thickness h_r^i. Thus, at each intersection of the curve with itself, there are two values of thickness producing the same color in the interference pattern. By omitting these points, we obtain the thickness values that produce unique colors [Fig. 7(b)]. It is clearly seen that the color database can be used to estimate film thickness ranging from 0.5 μm to 1 μm without ambiguity. Outside of this range, thickness measurements for individual points are not reliable. The entire profile, however, can be constructed if the smoothness and continuity of thickness profiles are taken into account.

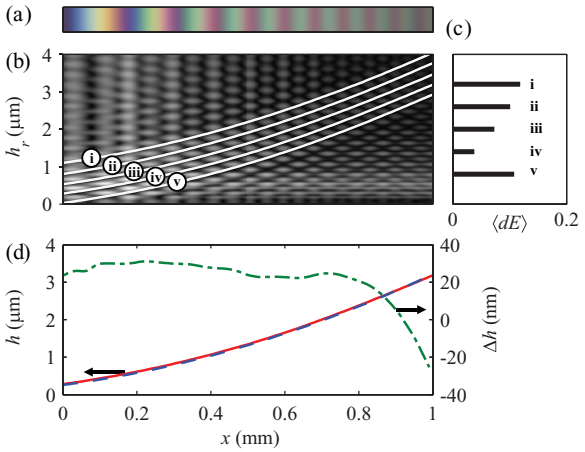

FIG. 8. (Color online) (a) A schematic of the setup for the test case in which a lens (surface radius $R = 300$ mm) is placed on top of a glass slide. (b) Color sample taken along a radial direction of a interference pattern. The origin $x = 0$ is not where the lens and the glass slide are in contact. (c) Color difference with candidate profiles in white solid lines. (d) Average color difference of candidate profiles shown in (c). The selected profile is profile (iv). (e) Comparison between the selected profile (shown in solid line) and the profile of the lens (shown in dashed line). The difference Δh (shown in dashed-dotted line) between the selected profile and the lens's profile.

APPENDIX B: A TEST CASE TO ASSESS THE METHOD'S ACCURACY

First, we generate an interference pattern from an air film between a glass slide and a lens. This arrangement is similar to the one used for color calibration but with a different lens (the radius of the lens used in this setup is 300 mm). From the resulting interference pattern, we exclude the part where two surfaces are in contact (correspondingly, the color is close to black) to simulate the real situations in which the liquid does not necessarily touch the solid surface. The film thickness that needs to be determined is within the range of the calibrated thickness. The interference pattern, after averaged azimuthally and expanded in the transverse direction, is the color sample shown in Fig. 8(a).

Using the method described in Sec. III, we decouple light intensity from the color sample and construct a grayscale plot of color difference between reference and sampled colors. The grayscale plot with candidate profiles of the air thickness are shown in Fig. 8(b). The profile with the smallest average color difference is then plotted against the profile of the lens used to generate the interference pattern [Fig. 8(d)]. As can be seen the difference between these profiles is no greater than 40 nm.

[1] A. M. Worthington, Proc. R. Soc. London **25**, 261 (1876).
[2] A. L. Yarin, Annu. Rev. Fluid Mech. **38**, 159 (2006).
[3] L. Xu, W. W. Zhang, and S. R. Nagel, Phys. Rev. Lett. **94**, 184505 (2005).
[4] M. M. Driscoll and S. R. Nagel, Phys. Rev. Lett. **107**, 154502 (2011).
[5] S. T. Thoroddsen, M.-J. Thoraval, K. Takehara, and T. G. Etoh, Phys. Rev. Lett. **106**, 034501 (2011).

[6] J. M. Kolinski, S. M. Rubinstein, S. Mandre, M. P. Brenner, D. A. Weitz, and L. Mahadevan, Phys. Rev. Lett. **108**, 074503 (2012).
[7] S. Mandre, M. Mani, and M. P. Brenner, Phys. Rev. Lett. **102**, 134502 (2009).
[8] M. Mani, S. Mandre, and M. P. Brenner, J. Fluid Mech. **647**, 163 (2010).
[9] P. D. Hicks and R. Purvis, J. Fluid Mech. **649**, 135 (2010).
[10] S. Mandre and M. P. Brenner, J. Fluid Mech. **690**, 148 (2012).
[11] S. Chandra and C. T. Avedisian, Proc. R. Soc. London A **432**, 13 (1991).
[12] S. T. Thoroddsen and J. Sakakibara, Phys. Fluids **10**, 1359 (1998).
[13] D. B. van Dam and C. Le Clerc, Phys. Fluids **16**, 3403 (2004).
[14] S. T. Thoroddsen, T. G. Etoh, K. Takehara, N. Ootsuka, and Y. Hatsuki, J. Fluid Mech. **545**, 203 (2005).
[15] T. Tran, H. J. J. Staat, A. Prosperetti, C. Sun, and D. Lohse, Phys. Rev. Lett. **108**, 036101 (2012).
[16] R. W. G. Hunt, *Measuring Colour* (Fountain Press, Kingston-Upon-Thames, 1998).
[17] C. Lin and R. F. Sullivan, IBM J. Res. Dev. **16**, 269 (1972).